

Phase Diagrams for Multi-Component Membrane Vesicles: A Coarse-Grained Modeling Study

Chen Zheng,[†] Ping Liu,[‡] Ju Li,[§] and Yong-Wei Zhang^{*‡}

[†]Department of Materials Science and Engineering, National University of Singapore, Singapore 119260,
[‡]Institute of High Performance Computing, Singapore 138632, and [§]Department of Materials Science and
Engineering, University of Pennsylvania, Pennsylvania 19104

Received February 24, 2010

We develop a multicomponent membrane coarse-grained model in which the effects of spontaneous curvature and fluidity are included. This model is used to perform computer simulations to study the phase segregation, domain coarsening, budding and budding off of multicomponent membrane vesicles. Three types of phase diagram are presented with variation of composition, spontaneous curvature, and line tension (the unlike bond energy). Various phases have been observed, including, sphere, biconcave, starfish, capsule, budding, and budding off. Our simulations show that budding off occurs only when the size of a domain is larger than a critical value, and the critical condition is closely related to the spontaneous curvature and line tension. A continuum model is used to predict the critical condition for budding off. Quantitative comparisons are made between the present simulation results and the continuum model predictions, and good agreements have been achieved.

1. Introduction

Biological membranes, which are composed of lipid molecules and proteins, play important roles in catalyzing numerous chemical reactions, mediating the transport of nutrients and wastes, and participating in signal sensing and transduction.^{1,2} The structures of biological membranes are dynamical in nature. For example, lipid molecules and proteins in the membrane systems are able to diffuse within membranes layers, and undergo phase aggregation, dispersion or separation.^{2–7} In addition, along the endocytic and biosynthetic–secretory pathways, the formation of vesicle through membrane budding and fission is a necessary step that ensures smooth production and transportation of biomolecules.¹

Cell or large vesicle may change its shape, volume, or surface area arising from a change in the properties of membrane itself and/or in the response to external stimulations. Various shapes of cells and vesicles have been reported in experiments, such as biconcave, starfish, budding, and pearling.^{8–16} Both continuum and atomistic methods have been used to simulate the behavior of cell membranes.

Apparently many mechanical and physical properties of lipid bilayer membranes are independent of the detailed molecular structures of membrane. Thus, many studies focused on the thermodynamic and energetic analyses based on continuum framework. It is believed that cell shapes are largely dictated by spontaneous curvature, line tension, and composition.^{12–15,17–20} A biological membrane is often described as a single-layer continuum membrane, which spans in a three-dimensional space. The seminal Helfrich theory is such a model based on the single-layer membrane assumption.²¹ This model has been widely used to understand the shaping energetics of cells and vesicles, and many insightful understandings have been achieved. Budding and domain shape transformation in mixed films and bilayer membranes was studied using the continuum Monge representation.¹⁷ The effect of line tension, spontaneous curvature, and component concentration was investigated. It was found that at high concentration, a transition occurs from circular domains to stripes while at high line tension, a transition occurs from circular domains to spherical buds. The stability of multicomponent membranes with planar topology as a function of membrane composition, spontaneous curvature of both components, and line tension was studied using a continuum model in the strong segregation limit.¹⁸ It was found that spontaneous curvature and line tension promote budding. Recent modeling and simulation work showed that asymmetric and curved component such as conical component can cluster together and form budding and vesiculation.^{19,20} An energy minimization method was used to study the polymorphism of vesicles with multidomain patterns.²⁰ The effect of bending rigidity, the Gaussian curvature moduli, and the line tension of the domain boundaries on the domain patterns and shapes was investigated. Various phases were found, and

*Corresponding author. Fax: 65 64674350. E-mail: zhangyw@ihpc.a-star.edu.sg.

(1) Lipowsky, R.; Sackmann, E. *Structure and Dynamics of Membranes*; Elsevier: Amsterdam, 1995.

(2) Bloom, M.; Evans, E.; Mouritsen, O. G. *Q. Rev. Biophys.* **1991**, *24*, 293–397.

(3) Rice, P. A.; McConnell, H. M. *Proc. Natl. Acad. Sci. U.S.A.* **1989**, *86*, 6445–6448.

(4) Benvegnu, D. J.; McConnell, H. M. *J. Phys. Chem.* **1992**, *96*, 6820–6824.

(5) Dekoker, R.; McConnell, H. M. *J. Phys. Chem.* **1994**, *98*, 5389–5393.

(6) Vist, M. R.; Davis, J. H. *Biochemistry* **1990**, *29*, 451–464.

(7) Almeida, P. F.; Vaz, W. L.; Thompson, T. E. *Biochemistry* **1992**, *31*, 6739–6747.

(8) Sackmann, E.; Duwe, H. P.; Engelhardt, H. *Faraday Discuss. Chem. Soc.* **1986**, *81*, 281–290.

(9) Duwe, H. P.; Käs, J.; Sackmann, E. *J. Phys. (Paris)* **1990**, *51*, 945–962.

(10) Bar-Ziv, R.; Moses, E. *Phys. Rev. Lett.* **1994**, *73*, 1392–1395.

(11) Baumgart, T.; Hess, S. T.; Webb, W. W. *Nature* **2003**, *425*, 821–824.

(12) Wintz, W.; Döbereiner, H. G.; Seifert, U. *Europhys. Lett.* **1996**, *33*, 403–408.

(13) Lim, G. H. W.; Wortis, M.; Mukhopadhyay, R. *Proc. Natl. Acad. Sci. U.S.A.* **2002**, *99*, 16766–16769.

(14) Seifert, U.; Berndl, K.; Lipowsky, R. *Phys. Rev. A* **1991**, *44*, 1182–1202.

(15) Jülicher, F.; Lipowsky, R. *Phys. Rev. E* **1996**, *53*, 2670–2683.

(16) Lipowsky, R. *J. Phys. II Fr.* **1992**, *2*, 1825–1840.

(17) Harden, J. L.; MacKintosh, F. C.; Olmsted, P. D. *Phys. Rev. E* **2005**, *72*, 011903.

(18) Gozdz, W. T.; Gompper, G. *Europhys. Lett.* **2001**, *55*, 587–593.

(19) Auth, T.; Gompper, G. *Phys. Rev. E* **2009**, *80*, 031901.

(20) Gutleider, E.; Gruhn, T.; Lipowsky, R. *Soft Matter* **2009**, *5*, 3303–3311.

(21) Helfrich, W. *Z. Naturforsch* **1973**, *28c*, 693–703.

these different multidomain patterns and vesicle shapes were summarized in terms of morphology diagrams.

It is noted that these continuum models have difficulties to address diffusive behavior, phase segregation, and fission and fusion of liquid membrane. Such issues can be naturally addressed using atomistic models. However, the membranes of cells and intracellular organelles contain a large number of amphiphilic lipid molecules. Currently it is impossible to perform full-scale molecular dynamics simulation of a large area of a lipid bilayer membrane by considering all the atoms. Conventionally coarse-grained models are used. So far, several coarse-grained models were developed to study membrane morphology and properties.^{22–46} Many interesting and valuable understandings have been achieved. For example, the dynamics of phase separation in multicomponent bilayer fluid vesicles was investigated using dissipative particle dynamics.²² The solvent particles were explicitly accounted for, and the effects of area-to-volume constraints were able to be included. Various regimes such as coalescence of flat patches, budding, vesiculation, and coalescence of caps were observed. Multipolar interactions between particles were included in dissipative particle dynamics simulations.²³ This inclusion enabled extended membrane structures emerging in a self-organized manner and exhibiting necessary mechanical stability for transport and membrane fluidity. Coarse-grained molecular dynamics simulations were used to study the effect of local curvature on aggregation and vesiculation of membrane proteins.²⁴ It was found that once a minimal local bending is realized, this local curvature can drive the protein cluster formation and subsequent transformation into vesicles. In addition, Monte Carlo method was also used to simulate the bilayer formation and budding dynamics of multicomponent membranes. Many interesting results such as budding through three distinct regimes²⁵ and the asymmetry of bilayer membrane during mixed amphiphile assembly³⁹ were obtained.

It should be noted that most of the models explicitly consider amphiphilic characteristics of the membrane molecules and explicitly consider the water molecules to stabilize the molecular

structures of the membrane. Thus, it is difficult to use them for large-scale (spatially and temporally) simulations. As a consequence, the modeling of the fluidic and diffusive behavior may not be possible due to the short simulation time scale. Hence the kinetic effect and cell morphology may not be realistically described. To overcome these difficulties, implicit solvent membrane models were proposed.^{40–46} These implicit solvent models were able to reproduce many membrane features observed experimentally, justifying the use of these implicit solvent models. However, most of these models either consider one-component membrane structure, or do not include the spontaneous curvatures. Thus, it is important to extend these models to consider multicomponent and spontaneous curvature. Since macroscopic properties of membranes cannot possibly depend on all the details of the atomic structures and description, even coarser-grained models are required for simulations with a larger spatial scale and longer time scale.

Phase diagram for vesicle topologies at different membrane properties and external loading conditions is able to reveal important thermodynamic behavior of cell membrane. So far the phase diagram for multicomponent vesicles has been only partially explored. For example, the phase diagram at different line tension and domain size was studied.¹⁵ However, the phase diagram concerning spontaneous curvature, line tension and composition has not been systematically studied.

Here, a coarse-grained model is proposed to describe multicomponent membranes. In the model, the adoption of directional degree without considering amphiphilicity of membrane molecules and solvent-free formulation allows us to perform large spatial- and temporal-scale simulations and to study fluidic and diffusive behavior of membranes. We perform coarse-grained molecular dynamics (CGMD) simulations to obtain the phase diagrams of multicomponent fluid vesicles and to reveal how spontaneous curvature, line tension, and composition affect the morphologies of vesicle. Various phases, such as, sphere, biconcave, starfish, capsule, budding, and budding off, are found with variation of spontaneous curvature, line tension, and composition. In addition, a simple energetic model is used to extract the invagination length and to predict the critical condition for budding off. The extracted invagination length and the predicted critical condition for budding off are consistent with our CGMD simulation results.

2. Model Formulation and Simulation Method

In the present work, we consider a multicomponent fluid membrane system. The membrane is assumed to consist of single-layered particle with a diameter of a_0 , which is also the membrane thickness. For particle i , 5 degrees of freedom are considered, that is, $(\mathbf{x}_i, \mathbf{n}_i)$, where \mathbf{x}_i is the position of particle i and \mathbf{n}_i is the surface normal vector at particle i subject to the constraint of $\mathbf{n}_i \cdot \mathbf{n}_i = 1$. Between particles i and j , $\mathbf{x}_{ij} = \mathbf{x}_j - \mathbf{x}_i$, its distance is $r_{ij} = |\mathbf{x}_{ij}|$ and unit vector $\bar{\mathbf{x}}_{ij} = \mathbf{x}_{ij}/r_{ij}$. The potential can be written as

$$V_{ij} = \begin{cases} \varepsilon \left(\frac{R_{cut} - r_{ij}}{R_{cut} - R_{min}} \right)^8 - 2\varepsilon \left(\frac{R_{cut} - r_{ij}}{R_{cut} - R_{min}} \right)^4 A(\mathbf{n}_i, \mathbf{n}_j, \bar{\mathbf{x}}_{ij}) & r_{ij} < R_{cut} \\ 0 & r_{ij} \geq R_{cut} \end{cases} \quad (1)$$

where, ε is the bonding energy, R_{cut} is the cutoff distance of the interaction, which is taken as $2.5a_0$, R_{min} is a parameter which is taken as $2^{1/6}a_0$, and $A(\mathbf{n}_i, \mathbf{n}_j, \bar{\mathbf{x}}_{ij})$ is a penalty function related to the

- (22) Laradji, M.; Sunil Kumar, P. B. *Phys. Rev. Lett.* **2004**, *93*, 198105.
 (23) Fuchslin, R. M.; Maeke, T.; McCaskill, J. S. *Eur. Phys. J. E* **2009**, *29*, 431–448.
 (24) Reynwar, B. J.; Ilyia, G.; Harmandaris, V. A.; Muller, M. M.; Kremer, K.; Deserno, M. *Nature* **2007**, *447*, 461–464.
 (25) Sunil Kumar, P. B.; Gompper, G.; Lipowsky, R. *Phys. Rev. Lett.* **2001**, *86*, 3911–3914.
 (26) Baoukina, S.; Monticelli, L.; Marrink, S. J.; Tieleman, D. P. *Langmuir* **2007**, *23*, 12617–12623.
 (27) Noguchi, H.; Takasu, M. *Biophys. J.* **2002**, *83*, 299–308.
 (28) Cooke, I. R.; Kremer, K.; Deserno, M. *Phys. Rev. E* **2005**, *72*, 011506.
 (29) Brannigan, G.; Lin, L. C. L.; Brown, F. L. H. *Eur. Biophys. J.* **2006**, *35*, 104–124.
 (30) Yamamoto, S.; Maruyama, Y.; Hyodo, S. *J. Chem. Phys.* **2002**, *116*, 5842–5849.
 (31) de Joannis, J.; Jiang, F. Y.; Kindt, J. T. *Langmuir* **2006**, *22*, 998–1005.
 (32) Drouffe, J. M.; Maggs, A. C.; Leibler, S. *Science* **1991**, *254*, 1353–1356.
 (33) Marrink, S. J.; Mark, A. E. *J. Am. Chem. Soc.* **2003**, *125*, 11144–11145.
 (34) Markvoort, A. J.; van Santen, R. A.; Hilbers, P. A. J. *J. Phys. Chem. B* **2006**, *110*, 22780–22785.
 (35) Noguchi, H.; Gompper, G. *Phys. Rev. E* **2006**, *73*, 021903.
 (36) Liu, P.; Li, J.; Zhang, Y. W. *Appl. Phys. Lett.* **2009**, *95*, 143104.
 (37) Deserno, M. *Macromol. Rapid Commun.* **2009**, *30*, 752–771.
 (38) Faller, R.; Marrink, S. J. *Langmuir* **2004**, *20*, 7686–7693.
 (39) Ji, S. C.; Ding, J. D. *Langmuir* **2006**, *22*, 553–559.
 (40) T. Snites, T.; Baumgartner, A. *Physica A* **1998**, *249*, 571–575.
 (41) Noguchi, H.; Takasu, M. *Phys. Rev. E* **2001**, *64*, 041913.
 (42) Farago, O. *J. Chem. Phys.* **2003**, *119*, 596–605.
 (43) Lenz, O.; Schmid, F. *J. Mol. Liq.* **2005**, *117*, 147–152.
 (44) Wang, Z. J.; Frenkel, D. *J. Chem. Phys.* **2005**, *123*, 154701.
 (45) Cooke, I. R.; Deserno, M. *J. Chem. Phys.* **2005**, *123*, 224710.
 (46) Revalee, J. D.; Laradji, M.; Sunil Kumar, P. B. *J. Chem. Phys.* **2008**, *128*, 035102.

deviation of instantaneous curvature from spontaneous curvature, and is taken as $1 + \gamma(B - 1)$, where B is taken as

$$B = \mathbf{n}_i \cdot \mathbf{n}_j - (\mathbf{n}_j \cdot \bar{\mathbf{x}}_{ij})(\mathbf{n}_i \cdot \bar{\mathbf{x}}_{ij}) + \beta_0(\mathbf{n}_j - \mathbf{n}_i) \cdot \bar{\mathbf{x}}_{ij} - \beta_0^2 \quad (2)$$

Here, γ is an energy penalty factor for the deviation of the membrane instantaneous curvature from its spontaneous curvature. From geometry analysis, the spontaneous curvature C_0 can be enforced if we choose $\beta_0 = r_{ij}C_0/2$.

The mechanical properties of a single-component membrane based on the above formulation but without the consideration of spontaneous curvature were studied.³⁶ It was found that the model was able to meet necessary requirements for mechanical stability and fluidity. The model was also used to simulate the shape transitions of vesicles with variation of pressure and temperature. Various morphologies of vesicles that were observed experimentally were obtained. For the single-component vesicle with spontaneous curvature, our simulation results show that the fluidic vesicle may break up into smaller vesicles, depending on the value of spontaneous curvature, temperature, and energy penalty factor.

In the present work, we include the spontaneous curvature and extend this model to describe a multicomponent system. For the like species interaction, namely a–a and b–b particle interaction, we choose the same ε and R_{\min} , i.e., $\varepsilon_{aa} = \varepsilon_{bb}$, $r_{\min}^{aa} = r_{\min}^{bb}$, but different C_0 . For the unlike species interaction, namely a-b particle interaction, we adopt the following mixing rule:⁴⁷ $r_{\min}^{ab} = (r_{\min}^{aa} + r_{\min}^{bb})/2$ and

$$\varepsilon_{ab} = \zeta \sqrt{\varepsilon_{aa}\varepsilon_{bb}}$$

It is noted that ε_{ab} is associated with line tension at domain boundaries. Under this mixing rule, the phase segregation occurs if ζ is smaller than one. Here the spontaneous curvature between particle a and particle b is taken as $(C_0^{(a)} + C_0^{(b)})/2$, where $C_0^{(a)}$ and $C_0^{(b)}$ are the spontaneous curvatures for the type-a particle membrane and the type-b particle membrane, respectively.

The governing equations of motion for particle i can be written as

$$m_i \ddot{\mathbf{x}}_i = -\frac{\partial V}{\partial \mathbf{x}_i} \quad (3)$$

$$\tilde{m}_i \ddot{\mathbf{n}}_i = -\frac{\partial V}{\partial \mathbf{n}_i} + \left(\frac{\partial V}{\partial \mathbf{n}_i} \cdot \mathbf{n}_i \right) \mathbf{n}_i - \tilde{m}_i (\mathbf{n}_i \cdot \mathbf{n}_i) \mathbf{n}_i \quad (4)$$

where \tilde{m}_i is a pseudomass, which is taken as $m_i a_0^2$. Solution of eq 4 guarantees that \mathbf{n}_i remains normal to the membrane surface and the constraint of $\mathbf{n}_i \cdot \mathbf{n}_i = 1$ is conformed.

The integration method proposed by Beeman⁴⁸ is used to solve eq 3 and eq 4. The position update algorithm is,

$$\mathbf{x}_{n+1} = \mathbf{x}_n + \mathbf{v}_n \Delta t + \frac{4\mathbf{x}_n - \mathbf{x}_{n-1}}{6} (\Delta t)^2 \quad (5a)$$

and that for velocity is

$$\mathbf{v}_{n+1} = \mathbf{v}_n + \frac{5\mathbf{x}_{n+1} + 8\mathbf{x}_n - \mathbf{x}_{n-1}}{12} \Delta t \quad (5b)$$

The Berendsen method⁴⁹ was used to maintain an approximately constant temperature during the simulations.

In the present simulations, the number of particles in a typical vesicle is 5072 and the initial radius of the vesicle R_0 is $20a_0$. Particles of different species are randomly distributed in the vesicle membrane and phase segregation is simulated starting from this initial condition. The spontaneous curvature of a membrane containing only type-a particles is taken to be 0, i.e. $C_0^{(a)} = 0$, while the spontaneous curvature of a membrane containing only type-b particles is $C_0^{(b)}$. The composition for type-a particles, x_a , is defined as

$$x_a = \frac{N_a}{N_a + N_b}$$

whereas the composition for type-b particles, x_b , is defined as

$$x_b = \frac{N_b}{N_a + N_b}$$

where N_a is the total number of type-a particles, and N_b is the total number of type-b particles. Apparently, $x_a + x_b = 1$. The energy penalty factor is chosen as $\gamma = 1.5$. The temperature is taken as $k_B T / \varepsilon = 0.2$, which is above the melting temperature of the membrane.³⁶ Therefore, the membrane is in liquid state. In the result presentation, the energy is normalized by ε ; and the length by a_0 . For the typical case, the CPU time on the 2.2 GHz AMD Opteron is about 70 h for the vesicle evolving from the initial homogeneous phase, through phase segregation, domain coarsening, budding and finally to budding-off.

3. Results and Discussion

In the present study, we focus on three system parameters: composition x_b , the spontaneous curvature of type-b particles $C_0^{(b)}$, and the unlike species interaction energy ε_{ab} . We will show that these three parameters are of great importance in controlling the morphology, phase segregation, budding and budding off of the multicomponent membrane vesicle.

3.1. The ε_{ab} - x_b Phase Diagram. Here we focus on the ε_{ab} - x_b phase diagram at a fixed spontaneous curvature value of

$$C_0^{(b)} = \frac{1}{5a_0}$$

Figure 1 shows the ε_{ab} - x_b phase diagram at

$$C_0^{(b)} = \frac{1}{5a_0}$$

There are three phase zones being observed. Figure 2a shows the initial random distribution of type-b particles in the vesicle (in this and following figures, type-a particles are in red and type-b particles are in green). Since the bonding energy between the unlike particle species is lower than that between the like particle species, phase segregation occurs as indicated in Figure 2b. At a small value of x_b , there is no budding, that is, only patch formation is observed. With further increasing x_b , the green domain starts to bud, followed by budding off at higher values of x_b . Examples are given in Figure 2(b), (c) and (d), which show the three different morphologies corresponding to $x_b = 0.1$, $x_b = 0.25$, and $x_b = 0.33$, respectively at a fixed value of $\varepsilon_{ab} = 0.66$. The evolution pathway for the budding off at $x_b = 0.33$ is shown in Figure 3a–d. At the early stage, large green buds are formed as shown in Figure 3a. These large buds grow in size by absorbing smaller green patches as shown in Figure 3b.

(47) Reszko-Zygmunt, J.; Patrykiewicz, A.; Sokolowski, S.; Sokolowska, Z. *Mol. Phys.* **2002**, *100*, 1905–1910.

(48) Beeman, D. J. *Comput. Phys.* **1976**, *20*, 130–139.

(49) Berendsen, H. J. C.; Postma, J. P. M.; Vangunsteren, W. F.; Dinola, A.; Haak, J. R. *J. Chem. Phys.* **1984**, *81*, 3684.

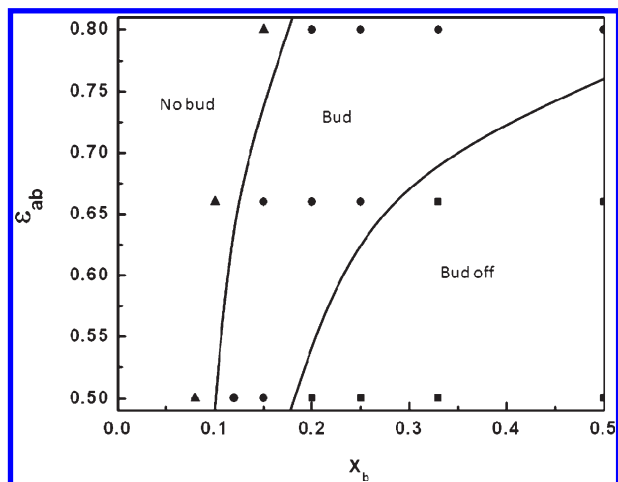


Figure 1. Phase diagram for vesicle topologies as a function of ε_{ab} and composition x_b at $C_0^{(b)} = 1/5a_0$. In total, three phases are identified. The dots correspond to the simulation cases.

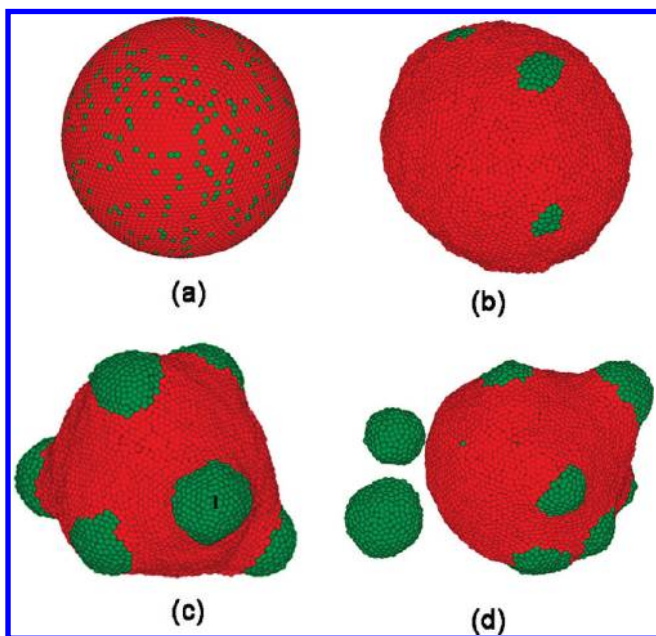


Figure 2. The initial configuration and three different morphologies in Figure 1 at $\varepsilon_{ab} = 0.66$. Key: (a) the initial configuration, (b) no bud, (c) bud, and (d) bud off.

Subsequently, these large green buds are able to pinch off as shown in Figure 3c and Figure 3d.

We have performed CGMD simulations with well-designed initial configurations to understand the interaction between different green domains. We find that when two buds are roughly at the equal size, they tend to repel and move away from each other to avoid the large curvature between them. For other cases, such as, one large bud and one small bud, one bud and one patch, and one patch and another patch, merge is observed. For example, we designed a vesicle with only two green domains with the same number of green particles. The number of particles for the domain is the same as that of bud “1” in Figure 2c. The gap between the two green domains is about a_0 as shown in Figure 4a. The two domains first form two buds, respectively as shown in Figure 4b, and then the two buds repel and move away from each other as shown in Figure 4c. Hence the buds with roughly the same size repel each other, and no merge is observed. Our energy

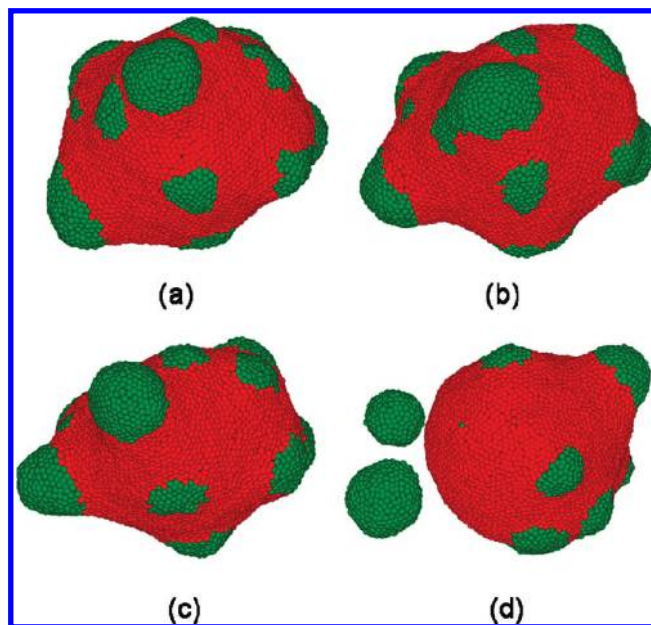


Figure 3. Snapshots for the buds and/patches merging and budding off. Through the merging, some of the buds reach a critical size, leading to budding off.

calculations show that the total system energy for Figure 4c is higher than a larger green domain merged by the two smaller domains, indicating that Figure 4c is only a metastable state. We also perform CGMD simulations for other cases. For example, Figure 5 shows two different green domains but with different sizes: The size of one of the green domains is the same as bud “1” in Figure 2c, while the number of particles for the other green domain is only 1/9 of the first. It can be seen that the two green domains merge as shown in Figure 5b, subsequently a large bud is formed in Figure 5c. These CGMD simulations suggest that the fusion of budding domains may not occur spontaneously because buds with a similar size tend to repel each other to avoid high curvature build-up between them. Hence it is concluded that the vesicle with buds as shown in Figure 2c is in a metastable state. Our simulations also explain the experimental observations of vesicles with relatively regular budding domains.¹¹

Our simulations strongly suggest that there is a critical size for budding off. Previous studies showed that a membrane domain may become unstable beyond a certain size and then undergo a budding or budding off.^{15,16} This instability is driven by the competition between bending energy of the domain and line energy of the domain boundary. For a vesicle with only two domains α and β , the bending energy of the vesicle can be written as¹⁵

$$E_{\text{bend}} = \int_{\alpha} dA \left[\frac{k^{(a)}}{2} (C_1 + C_2 - C_0^{(a)})^2 \right] + \int_{\beta} dA \left[\frac{k^{(b)}}{2} (C_1 + C_2 - C_0^{(b)})^2 \right] \quad (6a)$$

where C_1 and C_2 denote the two principal curvatures of membrane surface. $k^{(a)}$ and $k^{(b)}$ are the bending rigidities for domain α and domain β , respectively. $C_0^{(a)}$ and $C_0^{(b)}$ are spontaneous curvatures for the two domains. The edge energy of the vesicle is given by¹⁵

$$E_{\text{edge}} = \sigma L \quad (6b)$$

where σ is the line tension of the domain boundary and L is the length of the domain boundary. When the sum of the total

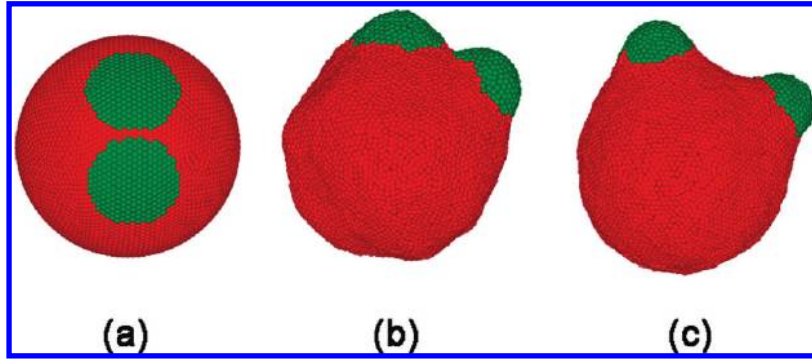


Figure 4. Snapshots for the evolution of a vesicle with two green domains initially in equal size at $\epsilon_{ab} = 0.66$. Both green domains form buds. The two buds repel and move away from each other to reduce the high curvature between them, forming metastable state.

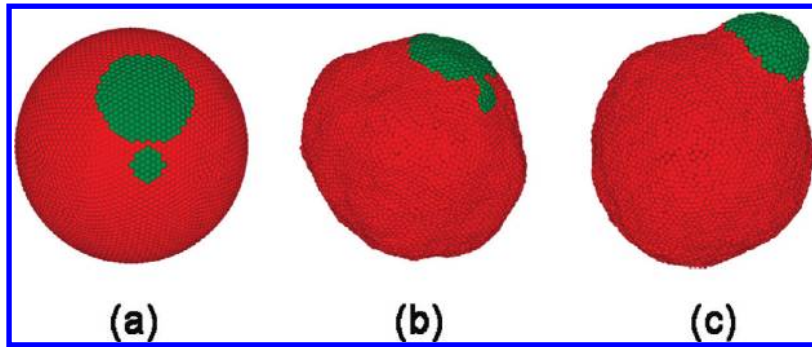


Figure 5. Snapshots for the evolution of a vesicle with two green domains initially in different size at $\epsilon_{ab} = 0.66$. The domains merge and form a single bud.

bending energy and edge energy reaches a minimum, the vesicle will be in a relatively stable state. The budding process leads to a limiting shape for which the bud is connected by an infinitesimal neck to the original vesicle. This neck can be characterized by a general relation for the principle curvatures of the adjacent membrane segments¹⁵

$$k^{(a)}M^{(a)} + k^{(b)}M^{(b)} = \frac{1}{2}(k^{(a)}C_0^{(a)} + k^{(b)}C_0^{(b)} + \sigma) \quad (7)$$

Here, $M^{(a)}$ and $M^{(b)}$ denote the mean curvatures of the two domains at the point where they form the ideal contact. Since

$$x \equiv \frac{A^{(b)}}{A^{(a)} + A^{(b)}} \equiv \frac{A^{(b)}}{4\pi R_0^2}$$

and $A^{(b)} = 4\pi R_0^2 x$ and $A^{(a)} = 4\pi R_0^2(1 - x)$, one has

$$M^{(b)} = 1/(R_0\sqrt{x})$$

and

$$M^{(a)} = 1/(R_0\sqrt{1-x})$$

If these expressions are substituted in the eq 7 and $k^{(a)} = k^{(b)} = k$, the critical x can be obtained by

$$\left(\frac{1}{\sqrt{1-x}} + \frac{1}{\sqrt{x}}\right) = \frac{1}{2}R_0\left(C_0^{(a)} + C_0^{(b)} + \frac{1}{\xi}\right) \quad (8)$$

where, ξ is the characteristic invagination length

$$\xi = \frac{k}{\sigma}$$

Since the surface area of the bud is the same as the critical domain area for budding off, the critical radius for the domain can be expressed as

$$L^0 = 2R_0\sqrt{x} \quad (x \leq 0.5) \quad (9)$$

For our simulation with multiple domains, it is observed that budding off occurs only when the size of the domains is larger than a critical value. After one domain buds off from a vesicle, the critical size for budding off can be roughly estimated using eq 8 and eq 9 if we treat the vesicle membrane as a homogeneous phase with the same property of the dominant composition. We will discuss this point in more details in the next section. It should be noted that ϵ_{ab} is related to line tension σ . The smaller ϵ_{ab} is, the larger σ is. From eq 8 and eq 9, it is seen that when σ increases (that is, ϵ_{ab} is decreased), ξ is decreased, causing L^0 to decrease. This is consistent with our CGMD simulation results. Quantitatively, our simulations also show that when ϵ_{ab} decreases from 0.66 to 0.5, L^0 decreases from $10.6a_0$ to $6.6a_0$ for cases with

$$C_0^{(b)} = \frac{1}{5a_0}$$

It is noted that both the present CGMD model and previous more sophisticated CGMD models^{22,23,25} are able to predict the phase separation, budding, and budding off, indicating that the present CGMD captures the correct membrane mechanical properties.

3.2. The $C_0^{(b)}-x_b$ Phase Diagram. We consider the $C_0^{(b)}-x_b$ phase diagram at a fixed value of $\epsilon_{ab} = 0.5$. The $C_0^{(b)}-x_b$ phase diagram is shown in Figure 6. In total, six phase zones (P1–P6) are observed. At a low x_b and a small $C_0^{(b)}$, the P1 phase with many green buds is observed as shown in Figure 7a. When x_b increases, the P2 phase with several green buds pinching off from the vesicle is preferred as shown in Figure 7b. When x_b becomes majority

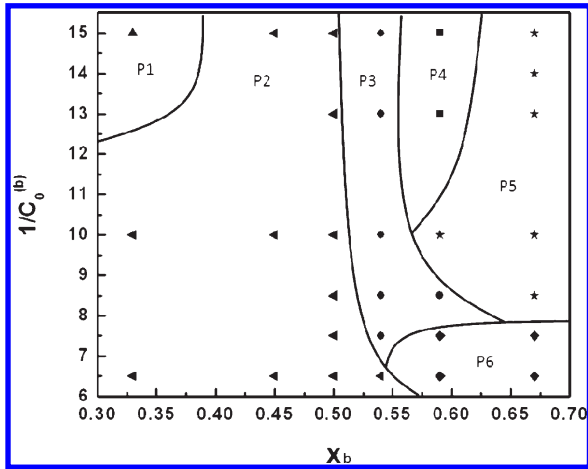


Figure 6. Phase diagram for vesicle topologies as a function of spontaneous curvature of the green domain and composition at $\varepsilon_{ab} = 0.5$. In total, six phases are observed. The dots correspond to the simulation cases.

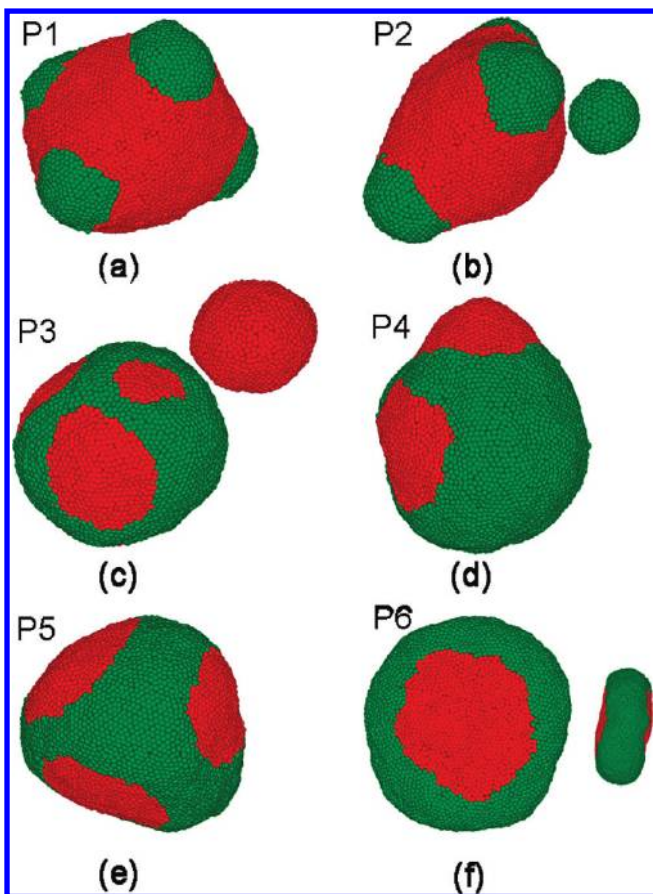


Figure 7. Vesicle shapes corresponding to the phase zones shown in Figure 6. Key: (a) P1 phase, vesicle with many green buds; (b) P2 phase, vesicle with a green bud off; (c) P3 phase, vesicle with a red bud off; (d) P4 phase, vesicle with red buds; (e) P5 phase, vesicle without buds; (f) P6 phase, vesicle with a biconcave shape.

(that is, $x_b > 0.5$), the P3 phase with one red bud pinching off is observed as shown in Figure 7c. With further increasing x_b , the P4 phase with one red bud is observed as shown in Figure 7d. However, there is no budding off in this case. With further increasing x_b while maintaining the value of $C_0^{(b)}$, the P5 phase without budding is observed as shown in Figure 7e. At an even higher x_b and a relatively large value of $C_0^{(b)}$, the P6 phase with a

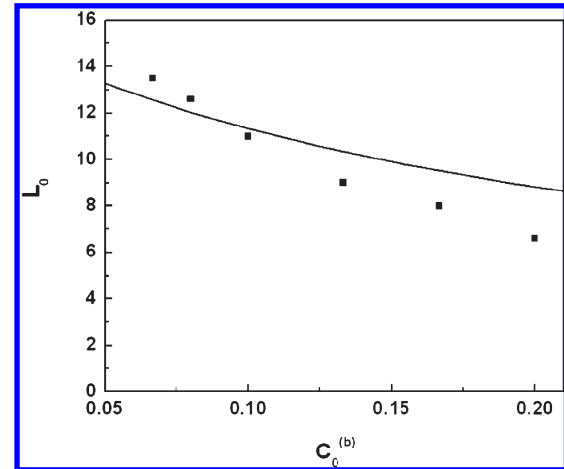


Figure 8. Variation of critical size with spontaneous curvature. The curve is obtained by the continuum model. The dots represent our simulation results with multiple domains using our CGMD model.

biconcave shape is observed as shown in Figure 7f. The smaller inset in Figure 7f shows the side view of the shape. Thus, the present simulation results show that the change in spontaneous curvature and composition can lead to complicated budding and budding off processes, which is consistent with the previous simulation works.^{17–20}

From Figure 6, it is seen that the spontaneous curvature strongly influences budding and budding off processes. For example, at $x_b = 0.33$, the green domain is able to bud at $C_0^{(b)} = 1/15a_0$, while the green domain budding off occurs at $C_0^{(b)} = 1/10a_0$. In addition, as can be seen from Figure 6, with a decrease of $C_0^{(b)}$ (or an increase of $1/C_0^{(b)}$), the budding off critical x_b for the green domain is increased. This trend is consistent with the prediction from eq 8 and eq 9.

Next, we would like to extract the invagination length and the line tension using eqs 8 and eq 9 and our CGMD simulation results. According to eq 8 and eq 9, L^0 increases when $C_0^{(b)}$ is decreased. For a given unlike bond energy ε_{ab} , the invagination length ξ can be extracted from eq 8. For example, for $\varepsilon_{ab} = 0.5$, we run cases, which initially only have two domains with $C_0^{(b)}$ equal to $1/5a_0$, $1/10a_0$, and $1/15a_0$, the observed critical x in our simulations is 0.05, 0.08, and 0.11, respectively; and the extracted invagination lengths are $2.8a_0$, $2.8a_0$, and $2.9a_0$ respectively. Hence the invagination length ξ is about $2.8a_0$. The bending rigidity k can be extracted by thermal fluctuation and its value is 1.78ε at $k_B T/\varepsilon = 0.2$.³⁶ Hence the line tension σ is $0.63\varepsilon/a_0$ or $2.2 \times 10^{-11} N$ at $\varepsilon_{ab} = 0.5$, which agrees well with literature values, which are in the order of $10^{-11} - 10^{-12}$.^{11,16} Figure 8 shows the comparison of the critical size L^0 obtained by using eq 9 and by our CGMD simulations. The curve represents the prediction of eq 8 and eq 9 at $\xi = 2.8a_0$ and the dots represent our simulation results at $\varepsilon_{ab} = 0.5$. It can be seen that the simulation results are in a reasonable agreement with the continuum model.

It is interesting to note that a green bud in Figure 7b pinches off while a red bud in Figure 7c pinches off. This implies again that the composition and spontaneous curvature play an important role in the budding off processes. Now we use eq 8 and eq 9 to explain the following four cases: (1) Why is there no budding off in Figure 7(a) with $x_b = 0.33$ and

$$C_0^{(b)} = \frac{1}{15a_0}$$

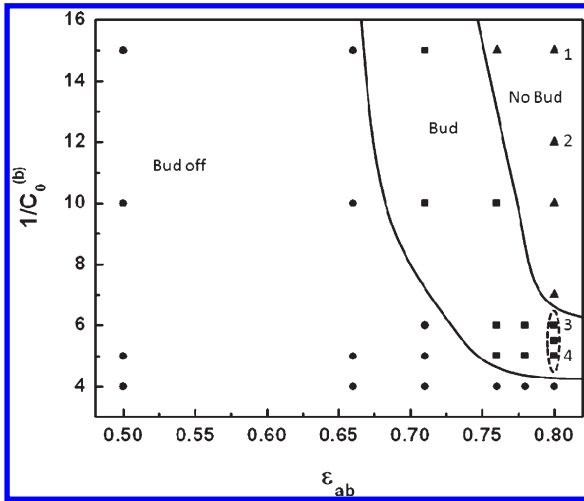


Figure 9. Phase diagram for vesicle topologies as a function of spontaneous curvature of the green domain and the unlike bond energy ε_{ab} at $x_b = 0.5$. In total, three phases are observed. The dots correspond to the simulation cases. The domain enclosed by the dot line indicates the bound for the formation of the starfish configurations.

(2) There is a green budding off in Figure 7b with $x_b = 0.45$ and

$$C_0^{(b)} = \frac{1}{15a_0}$$

(3) There is a red budding off in Figure 7c with $x_b = 0.54$ and

$$C_0^{(b)} = \frac{1}{15a_0}$$

(4) There is no budding off in Figure 7d with $x_b = 0.59$ and

$$C_0^{(b)} = \frac{1}{15a_0}$$

Since the only difference among the four cases is the composition and all other system parameters are the same, the critical size for budding off for the four cases should be the same. Using eq 8 and eq 9, and $C_0^{(a)} = 0$

$$C_0^{(b)} = \frac{1}{15a_0}$$

and $\xi = 2.8a_0$, it is found that the critical size for budding off is $12.6a_0$. We find that the size of the largest green bud in Figure 7a is about $11.8a_0$. Since the critical size is larger than the largest green bud size, therefore no budding off is observed. The diameter of the pinched off bud as shown in Figure 7b is roughly $13.6a_0$, which is larger than the critical size L^0 . Therefore, the green domain is able to bud off. Since the diameter of the red pinched off bud in Figure 7c is $20a_0$, which is also larger than the critical size, therefore the red domain is also able to bud off. For the red bud shown in Figure 7d, its size is $12.0a_0$, which is smaller than the critical size for budding off. Thus, no budding off occurs. Hence the continuum model (eq 8 and eq 9) is able to predict these complex processes observed in our CGMD simulations.

3.3. The $C_0^{(b)}-\varepsilon_{ab}$ Phase Diagram. Figure 9 shows the $C_0^{(b)}-\varepsilon_{ab}$ phase diagram at $x_b = 0.5$. Three phase zones (no budding, budding, and budding off) are observed. With increasing ε_{ab} , the configuration of the vesicle changes from bud off, to bud, and finally to no bud at relatively low values of $C_0^{(b)}$. Since an

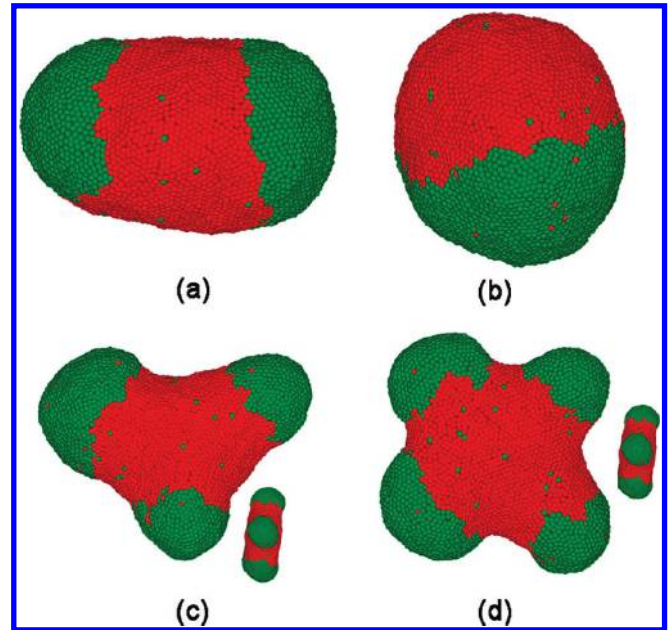


Figure 10. Vesicle shapes corresponding to the cases indicated in Figure 9 at $\varepsilon_{ab} = 0.8$. (a) corresponding to point 1, (b) corresponding to point 2, (c) corresponding to point 3, and (d) corresponding to point 4.

increase in ε_{ab} will cause a decrease in line tension, this will lead to an increase in critical size of the green domain for budding off according to eq 8. Therefore, the bud off for the green domain is only observed at low values of ε_{ab} and low values of $C_0^{(b)}$. Figure 10(a)-(d) show the four vesicle shapes at the same unlike bond energy $\varepsilon_{ab} = 0.8$. At $C_0^{(b)} = 1/15a_0$, the vesicle is in a capsule-like shape with two green domains at the two ends as shown in Figure 10a. At $C_0^{(b)} = 1/12a_0$, the vesicle is in a spherical shape with a red domain and a green domain each occupied half of the vesicle as shown in Figure 10(b). At $\varepsilon_{ab} = 0.8$, our simulation shows that ξ is about $7a_0$. For the configuration shown in Figure 10(b), since

$$Y = \frac{1}{2}R_0 \left(C_0^{(a)} + C_0^{(b)} + \frac{1}{\xi} \right)$$

$$= 2.3 \text{ at } C_0^{(a)} = 0,$$

$$C_0^{(b)} = \frac{1}{12a_0}$$

and $\xi = 7a_0$, the equation

$$\frac{1}{\sqrt{1-x}} + \frac{1}{\sqrt{x}} = 2.3$$

has no solution. Therefore, there is no bud off in Figure 10b. Again, the continuum model (eq 8 and eq 9) is able to predict these complex processes observed in our CGMD simulations.

Starfish configurations were observed in previous experiment.¹³ Here we show that starfish configuration can be obtained by changing the spontaneous curvature. Figure 10(c) displays a three-armed starfish which is observed at $C_0^{(b)} = 1/6a_0$. With increasing $C_0^{(b)}$ to $1/5a_0$, a four-armed starfish appears as shown in Figure 10d. With further increasing $C_0^{(b)}$, budding off of a green domain is observed instead the appearance of five or more armed starfish. Our simulations show that the starfish configurations occur only in a small regime for $C_0^{(b)}$ in between $1/6a_0$ and $1/4.5a_0$

at a low value of line tension as indicated by the domain enclosed by the dot line in Figure 9.

3.4. Discussion. Phase diagrams for vesicle topologies at different membrane spontaneous curvatures, compositions and the unlike bond energies have been computed by using the proposed CGMD model. It is shown that with variation of the system parameters, rich morphologies and topologies can be obtained. Overall, these morphologies and topologies are consistent with the various configurations of cells and vesicles, such as sphere, biconcave, starfish, capsule, budding, budding off and pearling, reported in experiments.¹³

Several comments can be made from the present work: (1) The present model is coarser than those which explicitly consider the bilayer structure of cell membranes^{22,24} and yet many important morphologies and topologies can be reproduced by the present model. The present work shows that many mechanical and physical properties of lipid bilayer membranes are independent of the detailed double molecular structures of membrane. (2) Many studies focused on the thermodynamic and energetic analyses based on continuum theories.^{17–20} These continuum theories were able correctly to predict that cell shapes are largely dictated by spontaneous curvature, line tension, and composition. However, membrane fluidity and diffusion are necessary for various biological functions of cells. These continuum models have difficulties to address diffusive behavior, phase segregation, and fission and fusion of liquid membranes. The present model exhibits necessary mechanical stability and membrane fluidity, providing a suitable tool to describe membrane kinetics in the context of coarse-grained cell biology. (3) In studying membrane morphology and dynamics, most of the models explicitly consider water molecules to stabilize the molecular structures of the membrane. The present work shows that a single-layer particle membrane can be effectively stabilized in a three-dimensional space by introducing the directional degrees of particles. This formulation significantly reduces the simulation complexity of membrane. (4) The complex morphologies and topologies obtained by the CGMD simulations can be reasonably explained by the simple energetic model elaborated above. The extracted invagination length and the predicted critical condition using the energetic model for budding off are consistent with our CGMD simulation results, indicating that thermodynamic factors are also in action. (5) Inclusion of spontaneous curvature in the present model allows us to fully explore its effect on the shape changes and budding dynamics. Our simulations show that spontaneous curvature plays an important role in membrane remodeling, such as endocytosis and vesiculation.

We would like to point out that biological membrane exhibits extraordinarily complex shapes, and the mechanisms by which these shapes are formed have not been fully understood. So far several mechanisms have been proposed for the generation of membrane curvature, for example, the change of surface-to-volume ratio, line tension, area-difference between the two leaflets, spontaneous curvature, membrane-associated proteins, and external forces.

The spontaneous curvature model and its variant allow the prediction of various cell and vesicle shapes. But the physical origin of the spontaneous curvature is not totally clear. Lipid bilayer membrane consisting of a lipid mixture is able to undergo phase separation into two different phases. This phase separation leads to the formation of numerous small domains, which accumulate and fuse into complicated patterns, suggesting the

existence of spontaneous curvature of the domains. An example is a mixture of phospholipids and cholesterol, which exhibits a broad coexistence region for two phases.^{6,11} Here we have adopted the spontaneous model as a simple representation for the membrane curvature. This model has allowed us to study the coupling of spontaneous curvature and phase segregation, and the evolution of shape of vesicles, and reveal many qualitative features of budding and budding off under the influence spontaneous curvatures. However, it is recognized that not all the features of shape changes can be predicted by spontaneous curvature models. When spontaneous curvature is absent in membrane, cell and vesicle shape changes can still be induced. This highlights that spontaneous curvature mechanism is just one of the mechanisms that control the membrane curvature. The area difference elasticity model is another one which also predicts various shapes of cells and vesicles. This area difference arises from the transbilayer asymmetry and the registry in two leaflets.^{39,50,51} The curvature-producing molecule model is another one which can also predict various membrane curvatures.⁵² Hence it is possible that the interplay among these mechanisms control the membrane curvature.⁵³

It should be noted that the present implicit solvent model is unable to control area-to-volume ratio, which has been shown to be important for cell shape changes. For example, homogeneous lipid membranes with periodic curvature modulation such as pearling states in tubular membranes and starfish vesicles have been observed by varying the surface-to-volume ratio.^{10,12} How to control the area-to-volume ratio under the framework of the implicit solvent model is an important future research work.

4. Conclusions

A CGMD model based upon our recent publication³⁶ was developed by including the spontaneous curvature, and a multi-component system was examined in this paper. The phase segregation, budding and budding off of multicomponent membrane vesicles were reproduced and investigated. The model adopted directional degree to consider amphiphilic nature of membrane molecule and solvent-free formulation, allowing us to perform large-scale simulations. In addition, the model can also describe the fluidic and diffusive behavior of membranes. Systematic CGMD simulations were performed to obtain partial phase diagrams by considering the effects of composition, spontaneous curvature, and line tension. Various shapes of vesicles were observed including, sphere, biconcave, starfish, capsule, budding, and budding off. We have also used the CGMD model to study the interactions between different buds or patches and convincingly demonstrated that vesicles with budding domains can be metastable due to the domain repulsion. Our simulations also show that there is a critical size for a domain to bud off. The critical condition is affected by the spontaneous curvature and line tension. A continuum model was used to predict the conditions for budding off under different conditions. Quantitative comparisons were attempted between the CGMD simulation results and the continuum model predictions, and good agreements were achieved.

(50) Sheetz, M. P.; Singer, S. J. *Proc. Natl. Acad. Sci. U.S.A.* **1974**, *71*, 4457–4461.

(51) Laradji, M.; Sunil Kumar, P. B. *Phys. Rev. E* **2006**, *74*, 040901(R).

(52) Zimmerberg, J.; Kozlov, M. M. *Nat. Rev. Mol. Cell Bio.* **2006**, *7*, 9.

(53) Boal, D. *Mechanics of the Cell*; Cambridge Univ. Press: Cambridge, U.K., 2002.